

Proton-Coupled Electron Transfer (PCET) with 1,4-Bisguanidino-Benzene Derivatives: Comparative Study and Use in Acid-Initiated C-H Activation

Petra Walter,^[a] Olaf Hübner,^[a] Elisabeth Kaifer,^[a] and Hans-Jörg Himmel^{*[a]}

Abstract: Proton-coupled electron transfer (PCET) is of key importance in modern synthetic chemistry. Redox-active guanidines were established by our group as valuable alternatives to toxic high-potential benzoquinones in a variety of different PCET reactions. In this work, the PCET reactivity of a series of 1,4-bisguanidino-benzenes varying in their redox potentials and proton affinities is evaluated. The relevant redox and protonation states are fully characterized, and the compounds sorted with respect to their PCET reactivity by comparative PCET experiments supplemented by quantum-chemical calculations. Depending on the studied reactions, the driving force is either electron transfer or proton transfer; thereby the influence of both processes on the overall

reactivity could be assessed. Then, two of the PCET reagents are applied in representative oxidative aryl-aryl coupling reactions, namely the intramolecular coupling of 3,3''-4,4''-tetramethoxy-*o*-terphenyl to give the corresponding triphenylene, the intermolecular coupling of *N*-ethylcarbazole to give *N,N'*-diethyl-3,3'-bicarbazole, and in the oxidative lactonization of 2-[(4-methoxyphenyl)methyl]-benzoic acid. Under mild conditions, the reactions proceed fast and efficient. Only small amounts of acid are needed, in clear contrast to the corresponding coupling reactions with traditional high-potential benzoquinones such as DDQ or chloranil requiring a large excess of a strong acid.

Introduction

Proton-coupled electron transfer (PCET) plays a central role in modern synthetic chemistry,^[1–4] as it allows for example the selective oxidation of organic compounds and other useful reactions.^[5–8] In biology, PCET is involved in essential processes such as photosynthesis and a variety of redox enzymatic reactions.^[9–13] The PCET chemistry of coordination compounds, for example oxo complexes of metals in high oxidation states, that are transformed in PCET reactions to hydroxy- or aqua-complexes,^[1] of metal oxide clusters such as the decatungstate anion $[W_{10}O_{36}]^{4-}$ ^[14] and of organic PCET reagents, for example quinones,^[15–18] TEMPO and other aminoxyl radicals,^[19–22] as well as Hantzsch esters and dihydropyridine derivatives,^[23,24] are well documented. By separating the electron acceptor/donor site from the proton acceptor/donor site, the two decisive parameters for the thermodynamics of PCET, the redox potential and the acid constant (proton affinity), could be tuned separately ("bidirectional" PCET).^[6–8,10]

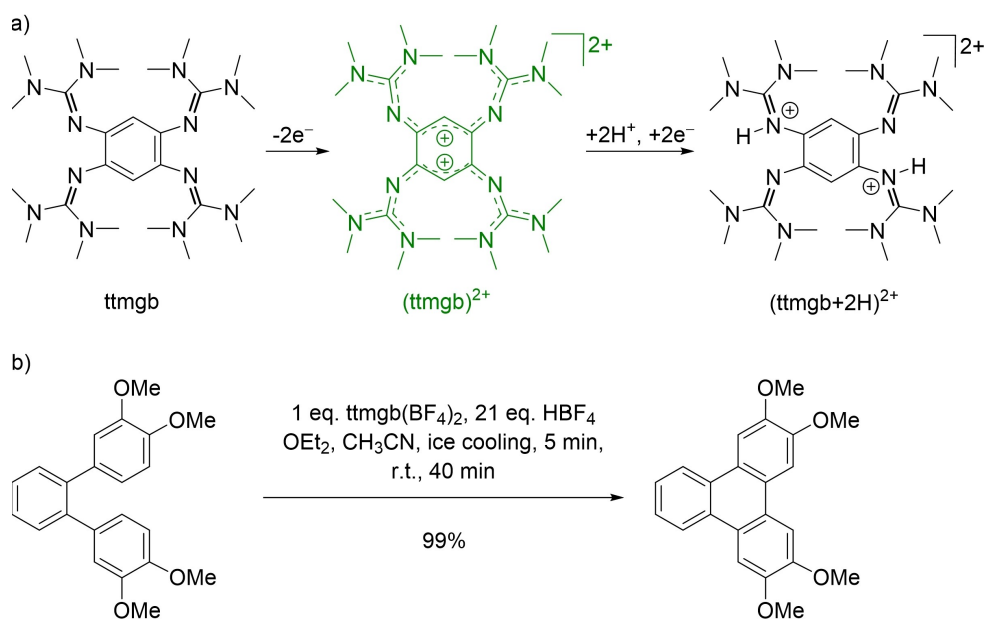
In the last years, our group established redox-active guanidines, comprising guanidino-functionalized aromatics (GFAs) and urea azines, as versatile organic PCET reagents and redox catalysts.^[25–30] The compound 1,2,4,5-tetrakis(tetramethylguanidino)-benzene (ttmgb, Scheme 1) is the archetypical example for a GFA,^[31,32] being an electron donor in its reduced, neutral state, but a remarkably potent oxidant in its oxidized, dicationic state, if electron transfer is coupled with proton transfer. Here, the high Brønsted basicity of the reduced, neutral state (pK_a ca. 25.3 for $(\text{ttmgb} + \text{H})^+$ in CH_3CN) contributes significantly to the driving force. The scope of the PCET reactivity of redox-active guanidines in organic synthesis could be greatly expanded in the presence of an excess of a strong acid. Hence, redox-active guanidines allow efficient aryl-aryl coupling reactions of aromatic compounds with relatively high redox potential up to at least 1.2 V vs. ferrocenium/ferrocene (Fc^+/Fc).^[29,30] Scheme 1 shows as example the conversion of 3,3'',4,4''-tetramethoxy-*o*-terphenyl (oxidation potential of 0.74 V vs. Fc^+/Fc) with one equivalent of $(\text{ttmgb})(\text{BF}_4)_2$ to the corresponding triphenylene coupling product in almost quantitative yield, requiring a large excess of a strong acid ($\text{HBF}_4 \cdot \text{OEt}_2$).^[29]

Recently we showed that oxidized bisguanidine 1,4-bis-(tetramethylguanidino)-benzene GFA1^{2+} (see Lewis structure in Figure 1a) is a stronger oxidant in PCET reactions than the oxidized tetrakisguanidine 1,2,4,5-tetrakis(tetramethylguanidino)-benzene, $(\text{ttmgb})^{2+}$.^[30] Therefore, it is attractive to study the PCET chemistry of redox-active bisguanidines in more detail. In this work, the PCET reactivity of the five different 1,4-bisguanidino-benzene derivatives sketched in Figure 1 is compared. Of these, GFA2, GFA4 and GFA5 are new, while GFA1^[33]

[a] P. Walter, Dr. O. Hübner, Dr. E. Kaifer, Prof. H.-J. Himmel
Inorganic Chemistry
Ruprecht-Karls University of Heidelberg
Im Neuenheimer Feld 270, 69120 Heidelberg (Germany)
E-mail: hans-jorg.himmel@aci.uni-heidelberg.de

Supporting information for this article is available on the WWW under <https://doi.org/10.1002/chem.202101539>

© 2021 The Authors. Chemistry - A European Journal published by Wiley-VCH GmbH. This is an open access article under the terms of the Creative Commons Attribution Non-Commercial License, which permits use, distribution and reproduction in any medium, provided the original work is properly cited and is not used for commercial purposes.



Scheme 1. a) Lewis structure of neutral ttmgb, twofold-oxidized green (ttmgb)²⁺ and reduced, twofold-protonated (ttmgb + 2H)²⁺. b) Example for an efficient and fast aryl-aryl coupling reaction with a salt of (ttmgb)²⁺.

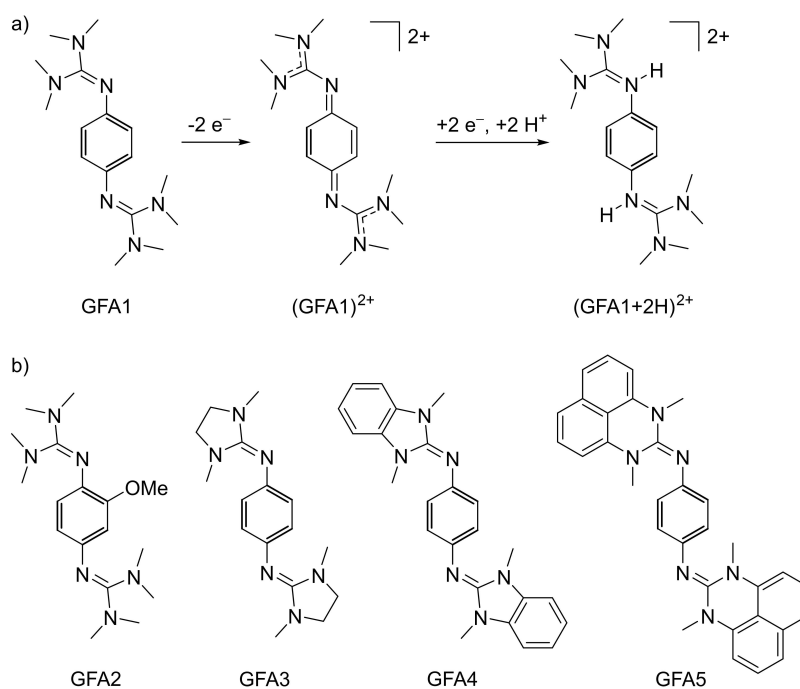
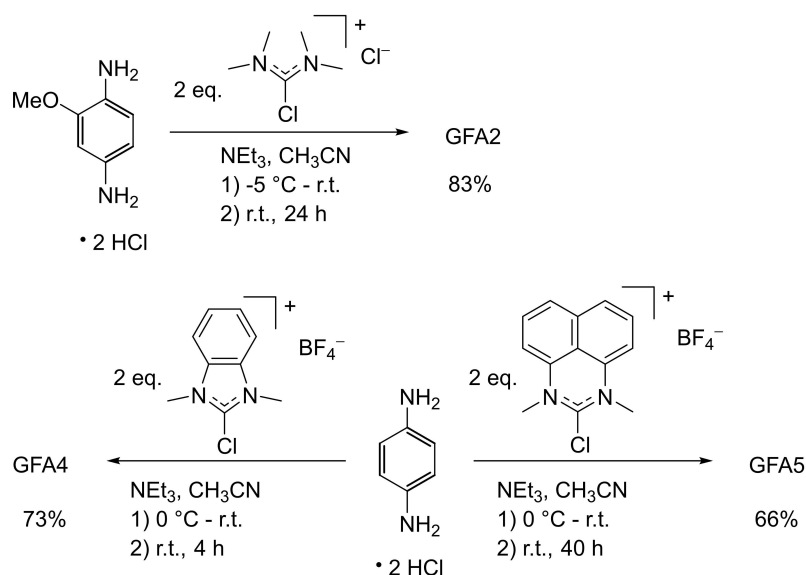


Figure 1. a) Conversion of the dicationic oxidized form, GFA1²⁺, in a (2e⁻, 2H⁺) proton-coupled electron transfer reaction to give the doubly protonated, reduced form, (GFA1 + 2H)²⁺. b) Selection of other redox-active guanidine ligands studied in this work. Of these, GFA2, GFA4 and GFA5 are new.

and GFA3^[30] were previously reported. In comparative (2e⁻, 2H⁺) PCET reactions, the oxidized GFA1²⁺ is reacted with the reduced, diprotonated form of another bis-guanidine. Depending on the guanidino groups, these reactions are either driven by electron-transfer (while proton transfer is unfavorable) or by proton-transfer (while electron-transfer is unfavorable); thereby, information about the reaction mechanism could be obtained

by comparing the PCET reactivity. Finally, GFA1²⁺ and GFA4²⁺ are applied as PCET reagents in representative intra- and intermolecular aryl-aryl coupling reactions, and in an oxidative lactonization. (The reasons for the choice of these two compounds is given below.) In sharp contrast to high-potential benzoquinones and also ttmgb, only a small amount of acid is required to initiate fast and efficient reactions.



Scheme 2. Synthesis of the three new redox-active bisguanidines GFA2, GFA4 and GFA5.

Results and Discussion

Synthesis and characterization

The three new bisguanidines GFA2, GFA4 and GFA5 were synthesized from the corresponding diamino precursors. Reaction of 2-methoxy-1,4-diaminobenzene^[34] with 2-chloro-1,1,3,3-tetramethylformamidine chloride gave GFA2. For the preparation of GFA4 and GFA5, 1,4-diaminobenzene was reacted with 2-chloro-1,3-dimethyl-1H-benzimidazol-3-ium tetrafluoroborate^[35] or 2-chloro-1,3-dimethylperimidinium tetrafluoroborate^[36] (Scheme 2).

Crystals of sufficient quality for structural analysis with single-crystal X-ray diffraction (XRD) were obtained for GFA2 and GFA4.^[37] Figure 2 illustrates the solid-state structures of the two new bisguanidines, and selected structural parameters are compiled in Tables 1 and 2. In line with the structures of other guanidino-substituted aromatics,^[25] the central CN₃ unit of each guanidino group is highly tilted with respect to the aromatic plane. A detailed analysis of this issue for GFA1 was published previously by our group,^[33] showing that this conformation is,

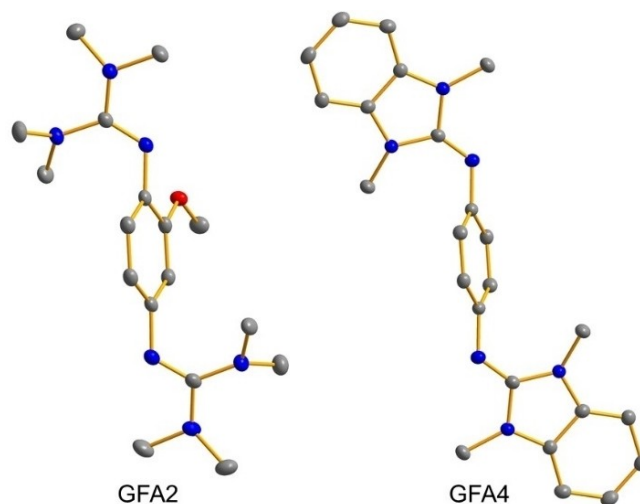


Figure 2. Illustration of the structures of the neutral bisguanidines GFA2 and GFA4 in the solid state. Displacement ellipsoids drawn at the 50% probability level. Hydrogen atoms omitted. Colour code: C grey, N blue, O red.

Table 1. Selected bond lengths (in Å) measured for GFA2 and (GFA2 + 2H)(PF₆)₂ in the solid state.^[37]

bond	GFA2	(GFA2 + 2H)(PF ₆) ₂
a	1.408(2)	1.422(2)
b	1.295(2)	1.350(2)
c	1.378(2)/1.390(2)	1.338(2)/1.330(2)
d	1.398(2)	1.386(2)
e	1.390(2)	1.385(3)
f	1.389(2)	1.389(2)
g	1.409(2)	1.398(2)
h	1.385(2)	1.389(2)
i	1.404(2)	1.404(2)

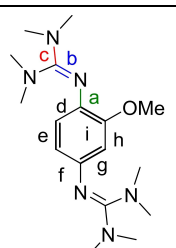
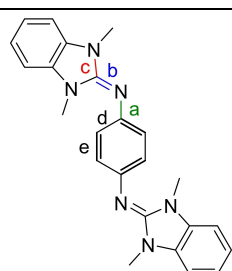


Table 2. Selected bond lengths (in Å) measured for GFA4, (GFA4 + 2H)(PF₆)₂ and GFA4(PF₆)₂ in the solid state.^[37]

bond	GFA4	(GFA4 + 2H)(PF ₆) ₂	GFA4(PF ₆) ₂
a	1.412(2)	1.421(2)	1.302(2)
b	1.287(2)	1.339(2)	1.376(3)
c	1.387(2)/1.391(2)	1.351(2)/1.349(2)	1.342(2)/1.345(2)
d	1.397(2)/1.400(2)	1.394(2)/1.392(2)	1.462(2)/1.451(3)
e	1.387(2)	1.386(2)	1.339(3)



for electronic reasons, highly favored energetically with respect to the conformation with co-planar CN₃ and aromatic planes.

Redox chemistry

Experimental results

Prior to chemical oxidation experiments, we carried out cyclic voltammetry to obtain information about the redox potentials. Figure 3 compares the cyclic voltammograms for the five GFAs studied in this work, and Table 3 summarizes the $E_{1/2}$ and E_{ox} values derived from these measurements. The curves for GFA1 - GFA4 were recorded in CH₂Cl₂ solutions. In the case of GFA5, the low solubility of the oxidized form hampered the determination of the redox potential in CH₂Cl₂ solution (dashed curve in Figure 3). Therefore, cyclic voltammetry measurements were repeated with the salt GFA5(PF₆)₂ of the oxidized form (see below for its synthesis and characterization) in CH₃CN solution (neutral GFA5 is poorly soluble in this solvent), yielding sharp waves due to a quasi-reversible two-electron redox process when the measurements started in reduction direction. The cyclic voltammograms of GFA1 and GFA2 clearly show a single reversible two-electron redox event; the first and the second electron are removed at equal potential. For GFA3, the waves are broader, signalling splitting of the two-electron redox process into two one-electron events with $E_{1/2}$ values of approximately -0.31 V for the redox couple GFA3^{•+}/GFA3⁰ and approximately -0.21 V for the redox couple GFA3²⁺/GFA3^{•+}. The potential separation of the two one-electron redox events increases for GFA4, with clearly separated $E_{1/2}$ values of -0.25 V for the redox couple GFA4^{•+}/GFA4⁰ and -0.06 V for the redox couple GFA4²⁺/GFA4^{•+}. From these values, one could estimate the disproportionation of GFA4^{•+} to GFA4 and GFA4²⁺ to be endergonic by 18 kJ mol⁻¹ with an equilibrium constant K_{disp} of $6.1 \cdot 10^{-4}$ (using the formula $\Delta G^0 = F \cdot \Delta E_{1/2}$ and $K_{disp} = \exp\{-[F/(RT)] \cdot \Delta E_{1/2}\}$).

Cyclic voltammetry measurements were also carried out in CH₃CN solution. The following redox potentials were obtained: $E_{1/2} = -0.21$ V ($E_{ox} = -0.18$ V) for GFA1, $E_{1/2} = -0.30$ V ($E_{ox} = -0.27$ V) for GFA2, $E_{1/2} = -0.24$ V ($E_{ox} = -0.20$ V) for GFA3, and (as already mentioned) $E_{1/2} = -0.15$ V ($E_{ox} = -0.12$ V) for GFA5. In all these cases, two-electron redox processes were found.

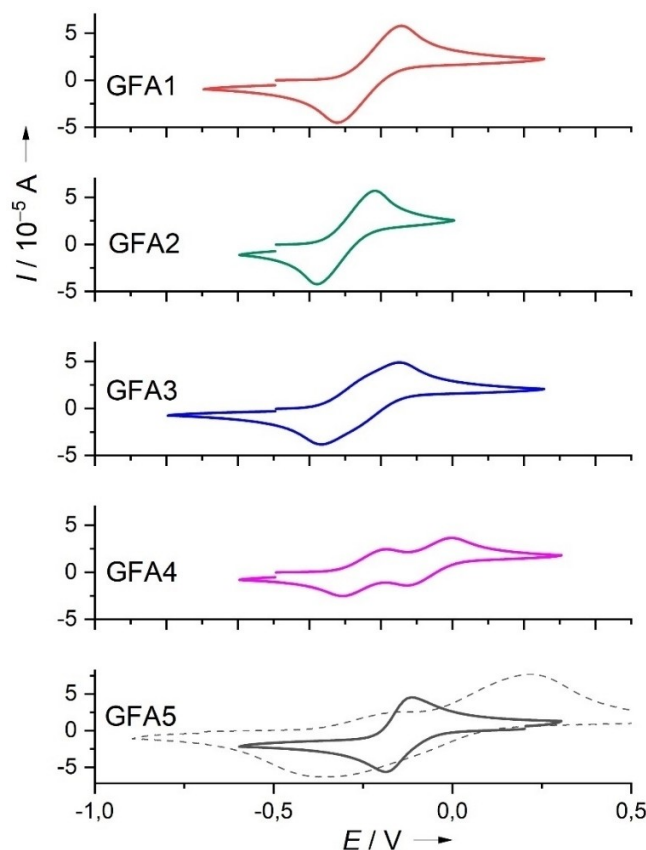


Figure 3. Comparison between the cyclic voltammograms in CH₂Cl₂ solution (Ag/AgCl reference electrode, 0.1 M (nBu)₄NPF₆ as supporting electrolyte, scan speed 100 mV s⁻¹) for the five redox-active guanidines discussed in this work. Potentials given with respect to the ferrocenium/ferrocene (Fc⁺/Fc) redox couple. In the case of GFA5, the dashed curve was obtained when measuring the CV for a CH₂Cl₂ solution of GFA5 in direction of oxidation, and the solid curve for measuring a CH₃CN solution of GFA5(PF₆)₂ (synthesis see below) in the direction of reduction.

However, in the case of GFA4, the low solubility in CH₃CN prohibited measurements in this solvent.

Two electrons and two protons are exchanged in PCET reactions between the dicationic, oxidized form of one and the doubly-protonated, reduced form of the other bisguanidine (see below). Therefore the value $-F[(E_{1/2}(1^{st}) + E_{1/2}(2^{nd}))]$ was calculated to compare the two-electron acceptor properties,

Table 3. $E_{1/2}$ and E_{ox} values (in V vs. the Fc^+/Fc couple) from cyclic voltammetry measurements in CH_2Cl_2 solution (Faraday constant $F = 9.648456 \cdot 10^4 \text{ C mol}^{-1}$).

Compound	1 st redox ($GFA^{\bullet+}/GFA^0$) $E_{1/2}(1^{st})/E_{ox}$	2 nd redox ($GFA^{2+}/GFA^{\bullet+}$) $E_{1/2}(2^{nd})/E_{ox}$	$-F[(E_{1/2}(1^{st}) + E_{1/2}(2^{nd}))]$ ($GFA^{2+} + 2 e^- \rightarrow GFA$)
GFA1	-0.23/-0.14	-0.23/-0.14	+44.4 kJ mol^{-1}
GFA2	-0.30/-0.22	-0.30/-0.22	+57.9 kJ mol^{-1}
GFA3	-0.31/-0.27	-0.21/-0.14	+50.2 kJ mol^{-1}
GFA4	-0.25/-0.18	-0.06/0.00	+29.9 kJ mol^{-1}
GFA5 ^[a]	-0.15/-0.12	-0.15/-0.12 V	+28.9 kJ mol^{-1}

[a] Measurements for $GFA5(PF_6)_2$ in CH_3CN due to low solubility in CH_2Cl_2 .

leading to the order for increasing “two-electron acceptor strength” (decreasing $-F[(E_{1/2}(1^{st}) + E_{1/2}(2^{nd}))]$ value): $GFA2 < GFA3 < GFA1 < GFA4 < GFA5$.

Chemical oxidation was carried out with two equivalents of $Fc(PF_6)$. In all cases, the products of two-electron oxidation were isolated as stable, storable solid compounds. Figure 4 illustrates the solid-state structures of the new compounds $GFA4(PF_6)_2$

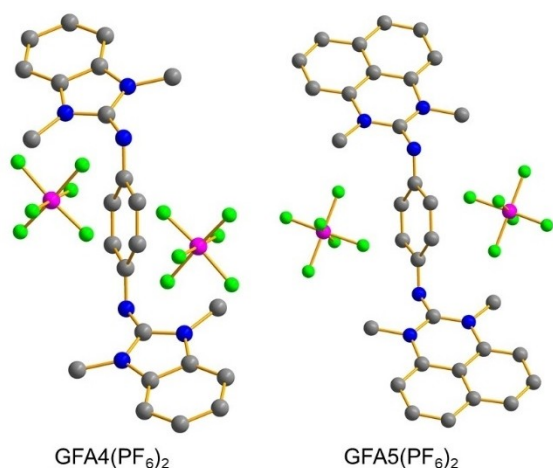


Figure 4. Illustration of the solid-state structures of the bisguanidine dicationic species $GFA4^{2+}$ and $GFA5^{2+}$, together with two PF_6^- counterions, obtained upon oxidation of the neutral compounds. Displacement ellipsoids drawn at the 50% probability level. Hydrogen atoms omitted. Colour code: C grey, N blue, P red, F green.

and $GFA5(PF_6)_2$.^[37] Selected bond lengths are included in Tables 2 and 4. As expected, the $N=C$ imino bond length of the neutral GFA increases significantly upon oxidation (e.g. from 1.287(2) Å in GFA4 to 1.376(3) Å in $GFA4(PF_6)_2$). By contrast, the $N-C$ bond connecting the guanidino group to the aromatic ring decreases (from 1.412(2) Å in GFA4 to 1.302(2) Å in $GFA4(PF_6)_2$). The large differences in the $C-C$ bond lengths within the C_6 ring of the oxidized molecules signal loss of the aromatic system, in line with the Lewis structure shown for $GFA1^{2+}$ in Figure 1.

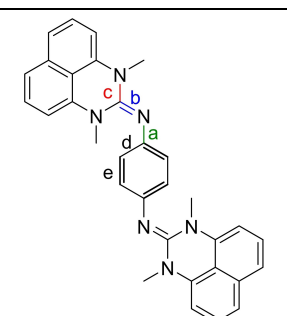
Finally, we prepared 1:1 mixtures between a neutral bisguanidine and the salt of the corresponding doubly-oxidized compound in CH_3CN solution and recorded UV-vis as well as EPR spectra. The appearance of an EPR signal and strong new absorptions in the visible region of the UV-vis spectra indicated the presence of the radical monocationic bisguanidine in significant amount, formed in a comproportionation reaction (despite of the absence of any sign of one-electron redox processes in the cyclic voltammograms). For example, Figure 5 displays the UV-vis spectrum of the green 1:1 mixture of GFA4 and $GFA4(PF_6)_2$, showing strong bands centered at 699 nm (very broad) and 426 nm that are absent in the spectrum of GFA4 or $GFA(PF_6)_2$ alone. Moreover, the inset shows the EPR spectrum measured for this mixture (broad, unstructured signal at $g=2.00$). TD-DFT calculations (B3LYP/def2-TZVP) predicted strong electronic transitions at 718 and 386 nm (Figure 6), in excellent agreement with the experiment. Plots of the isodensity surfaces for the orbitals involved in the transition at 718 nm are included in Figure 6, being π -orbitals delocalized over the complete molecule.

In the case of the radical monocation $GFA3^{\bullet+}$, prepared similarly by mixing equimolar amounts of GFA3 and $GFA3(PF_6)_2$, bands at 575 nm (with a shoulder at 542 nm) and 404 nm appeared.^[30] Here, TD-DFT calculations (B3LYP/def2-TZVP) predicted electronic transitions at 543/501 and 365/346 nm, again in good agreement with the experimental values (see Figure 6). The blue shift of the lowest-energy absorption of $GFA3^{\bullet+}$ compared to $GFA4^{\bullet+}$ could be explained by the reduced size of the π -electron system.

All 1:1 mixtures between the neutral and dicationic redox states showed EPR signals assigned to the radical monocations. In the case of $GFA1^{\bullet+}$ and $GFA5^{\bullet+}$, a distinct hyperfine coupling (HFC) to hydrogen and nitrogen nuclei is visible (Figure 7), with

Table 4. Selected bond lengths (in Å) measured for $(GFA5 + 2H)(PF_6)_2$ and $GFA5(PF_6)_2$ in the solid state.^[37]

bond	$(GFA5 + 2H)(PF_6)_2$	$GFA5(PF_6)_2$
a	1.429(2)	1.288(6)
b	1.349(2)	1.366(6)
c	1.346(2)/1.347(2)	1.342(6)/1.339(6)
d	1.391(2)/1.386(2)	1.460(6)/1.470(7)
e	1.389(2)	1.336(7)



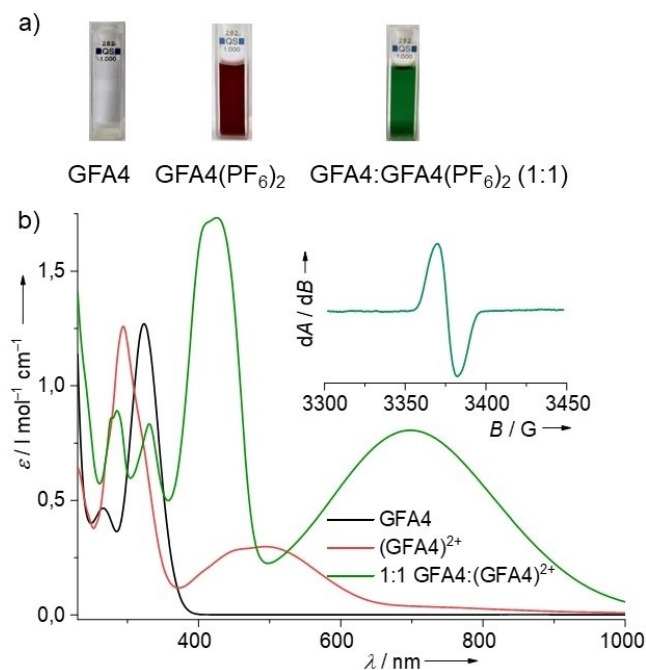


Figure 5. a) From left to right: Photos of cuvettes with CH_3CN solutions of GFA4, $\text{GFA4}(\text{PF}_6)_2$ and an equimolar mixture of GFA4 and $\text{GFA4}(\text{PF}_6)_2$. b) UV-vis spectra of GFA4, $\text{GFA4}(\text{PF}_6)_2$ and an equimolar mixture of GFA4 and $\text{GFA4}(\text{PF}_6)_2$ in CH_3CN solutions. The EPR spectrum of the 1:1 mixture in CH_2Cl_2 is shown in the inset.

a line spacing of 1.8 G. For the other radical monocations, the HFC is not clearly resolved and hidden under broad, unstructured signals. The presence of more than 20 lines indicates hyperfine coupling to the four equivalent aromatic H atoms and the two equivalent N atoms directly attached to the C_6 ring, producing in theory $(2 \cdot 2 \cdot 1 + 1)(2 \cdot 4 \cdot 1/2 + 1) = 25$ lines.

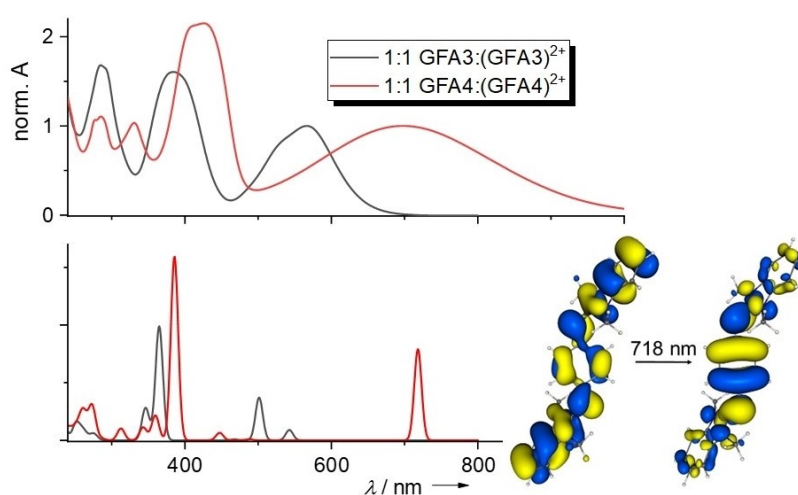


Figure 6. Comparison between the UV-vis spectra of 1:1 mixtures of GFA3 and $\text{GFA3}(\text{PF}_6)_2$ (black curve) and of GFA4 and $\text{GFA4}(\text{PF}_6)_2$ (red curve) in CH_3CN solutions. The spectra were normalized to the maximum of absorption of the lowest-energy transition. Simulations of spectra for GFA3^{3+} and GFA4^{3+} on the basis of TD-DFT calculations (B3LYP/def2-TZVP) are reproduced below the experimental spectra. In addition, isodensity plots for the two orbitals involved in the lowest-energy electronic transition of GFA4^{3+} at 718 nm are plotted (SOMO to LUMO transition, $52a_u(\text{beta}) \rightarrow 53a_u(\text{beta})$).

Quantum-chemical studies

Structures and electronic energies were calculated with the B3LYP functional together with the def2-TZVP basis set, since this combination was shown to give reliable results in previous studies with redox-active guanidines.^[27,29,30] Thermal contributions were calculated with the B3LYP functional and SV(P) basis set. The solvent effect was considered with the conductor-like screening model (COSMO), with a relative permittivity $\epsilon_r = 37.5$ (CH_3CN). (See Supporting Information for more details.) The calculations reproduced accurately the experimental solid-state structures (see Supporting Information for details). The thermodynamics calculated for the pure electron transfer reactions between the oxidized form $\text{GFA1}(\text{PF}_6)_2$ and one of the neutral, reduced bisguanidines GFA2-GFA5 (the anions were included in the calculations^[30]) are compiled in Table 5. For GFA2 and GFA3, the Gibbs free reaction energies are negative, meaning that they are stronger two-electron donors than GFA1. This result is in line with the cyclic voltammetry measurements for which the term $-F \cdot [(E_{1/2}(1^{\text{st}}) + E_{1/2}(2^{\text{nd}}))]$, being approximately the standard Gibbs free energy change for the reaction $\text{GFA}^{2+} + 2 e^- \rightarrow \text{GFA}$, is more positive for GFA2 and GFA3 than for GFA1. By contrast, the Gibbs free reaction energies are positive for GFA4 and GFA5, again in line with the results of the cyclic voltammetry measurements, showing that GFA4 and GFA5 are weaker two-electron donors than GFA1.

Protonation

Experimental results

All guanidines could be doubly protonated with two equivalents of NH_4PF_6 . The new salts $(\text{GFA2} + 2\text{H})(\text{PF}_6)_2$, $(\text{GFA4} + 2\text{H})(\text{PF}_6)_2$ and $(\text{GFA5} + 2\text{H})(\text{PF}_6)_2$ were crystallized from concen-

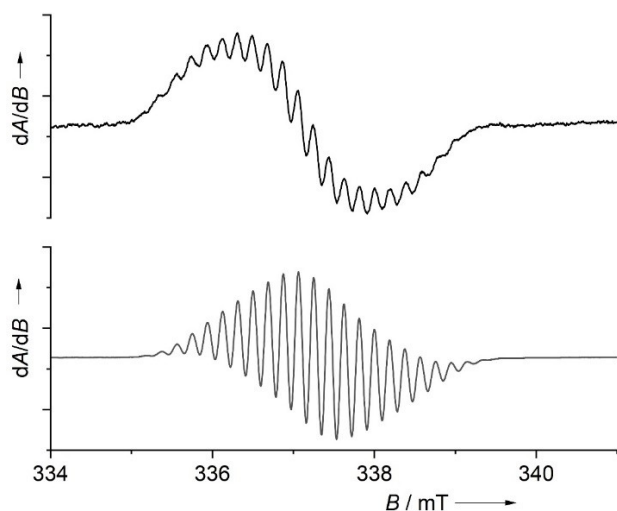


Figure 7. EPR spectra of the radical monocations GFA1^{*+} and GFA5^{*+} , formed from 1:1 mixtures of GFA1^{2+} and GFA1 and of GFA5^{2+} and GFA5 , respectively, in CH_2Cl_2 solutions (concentrations ca. $5 \cdot 10^{-3} \text{ mol} \cdot \text{L}^{-1}$) at room temperature.

Table 5. Calculated electronic energy, enthalpy at 0 K and Gibbs free energy at 298 K for pure electron transfer reactions (B3LYP functional in combination with the stated basis set, solvent effect modelled with the conductor-like screening model (COSMO)). Anions included in the calculations.

	$\epsilon_r = 1$	$\epsilon_r = 37.5$	
$\text{GFA1}(\text{PF}_6)_2 + \text{GFA2} \rightarrow \text{GFA1} + \text{GFA2}(\text{PF}_6)_2$	SV(P)	TZVP ^[a]	TZVP ^[a]
$\Delta_r E$	-65.7	-54.1	-28.4
$\Delta_r H_0$	-59.9	-48.2	-22.6
$\Delta_r G_{298}$	-53.1	-41.5	-15.9
$\text{GFA1}(\text{PF}_6)_2 + \text{GFA3} \rightarrow \text{GFA1} + \text{GFA3}(\text{PF}_6)_2$	SV(P)	TZVP ^[a]	TZVP ^[a]
$\Delta_r E$	-44.1	-39.3	-15.4
$\Delta_r H_0$	-44.4	-39.5	-15.6
$\Delta_r G_{298}$	-45.6	-40.8	-16.9
$\text{GFA1}(\text{PF}_6)_2 + \text{GFA4} \rightarrow \text{GFA1} + \text{GFA4}(\text{PF}_6)_2$	SV(P)	TZVP ^[a]	TZVP ^[a]
$\Delta_r E$	-10.9	-10.8	+11.8
$\Delta_r H_0$	-13.0	-12.8	+9.7
$\Delta_r G_{298}$	-6.7	-6.5	+16.0
$\text{GFA1}(\text{PF}_6)_2 + \text{GFA5} \rightarrow \text{GFA1} + \text{GFA5}(\text{PF}_6)_2$	SV(P)	TZVP ^[a]	TZVP ^[a]
$\Delta_r E$	-1.6	-1.9	+24.6
$\Delta_r H_0$	-4.8	-5.1	+21.4
$\Delta_r G_{298}$	-0.6	-0.9	+25.6

[a] Zero-point energy and thermal contributions calculated with the SV(P) basis set.

trated CH_3CN solutions layered with Et_2O . Figure 8 illustrates the XRD structures in the solid state;^[37] selected bond lengths are included in Tables 1, 2 and 4. As expected, protonation occurs exclusively at the imino N atoms and leads to an elongation of the imino $\text{N}=\text{C}$ bond lengths (e.g. from 1.295(2) Å to 1.350(2) Å upon protonation of GFA2 , and from 1.287(2) Å to 1.339(2) Å upon protonation of GFA4) that could be rationalized by charge delocalization through π -bonding over the three nitrogen

atoms and the central carbon atom of the protonated guanidino group.

Quantum-chemical studies

Unfortunately, the experimental determination of the Brønsted basicity from titration experiments is hampered by protonation equilibria and poorly resolved protonation steps in both the NMR and UV-vis spectra. Therefore, we first calculated the absolute proton affinities (at $\epsilon_r = 1$) for the five bisguanidines. Here, the order of increasing proton affinity is $\text{GFA5} < \text{GFA4} < \text{GFA3} < \text{GFA1} < \text{GFA2}$ (Table 6). In another calculation, the proton transfer between GFA1 and GFA2 was calculated with inclusion of PF_6^- counterions (reaction $(\text{GFA1} + \text{H})\text{PF}_6 + \text{GFA2} \rightarrow \text{GFA1} + (\text{GFA2} + \text{H})\text{PF}_6$). Interestingly, the PF_6^- counterions had a considerable influence on the thermodynamics. While $\Delta_r G_{298}$ for the reaction $(\text{GFA1} + \text{H})^+ + \text{GFA2} \rightarrow \text{GFA1} + (\text{GFA2} + \text{H})^+$ is negative ($-21.1 \text{ kJ mol}^{-1}$), it is slightly positive ($+3.5 \text{ kJ mol}^{-1}$) for the reaction $(\text{GFA1} + \text{H})\text{PF}_6 + \text{GFA2} \rightarrow \text{GFA1} + (\text{GFA2} + \text{H})\text{PF}_6$. It should be noted that the starting structures for the calculations were obtained by removal of one of the protons

Table 6. Electronic energy, enthalpy at 0 K and Gibbs free energy at 298 K for monoprotonation of the bisguanidines calculated with density functional calculations with the B3LYP functional and the stated basis set. The table also includes the thermodynamics for proton transfer from GFA1 to GFA2 in which the PF_6^- counterions were included.

$\text{GFA1} + \text{H}^+ \rightarrow (\text{GFA1} + \text{H})^+$	SV(P)	TZVP ^[a]
$\Delta_r E$	-1104.1	-1110.0
$\Delta_r H_0$	-1065.0	-1071.0
$\Delta_r G_{298}$	-1038.1	-1044.0
$\text{GFA2} + \text{H}^+ \rightarrow (\text{GFA2} + \text{H})^+$	SV(P)	TZVP ^[a]
$\Delta_r E$	-1123.6	-1129.5
$\Delta_r H_0$	-1084.2	-1090.1
$\Delta_r G_{298}$	-1059.2	-1065.1
$(\text{GFA1} + \text{H})\text{PF}_6 + \text{GFA2} \rightarrow \text{GFA1} + (\text{GFA2} + \text{H})\text{PF}_6$	SV(P)	TZVP ^[a]
$\Delta_r E$	+3.8	+3.0
$\Delta_r H_0$	+3.0	+2.2
$\Delta_r G_{298}$	+4.3	+3.5
$\text{GFA3} + \text{H}^+ \rightarrow (\text{GFA3} + \text{H})^+$	SV(P)	TZVP ^[a]
$\Delta_r E$	-1093.7	-1098.5
$\Delta_r H_0$	-1056.9	-1061.7
$\Delta_r G_{298}$	-1032.6	-1037.4
$\text{GFA4} + \text{H}^+ \rightarrow (\text{GFA4} + \text{H})^+$	SV(P)	TZVP ^[a]
$\Delta_r E$	-1075.1	-1082.8
$\Delta_r H_0$	-1038.6	-1046.3
$\Delta_r G_{298}$	-1012.4	-1020.0
$\text{GFA5} + \text{H}^+ \rightarrow (\text{GFA5} + \text{H})^+$	SV(P)	TZVP ^[a]
$\Delta_r E$	-1064.0	-1074.5
$\Delta_r H_0$	-1027.7	-1038.2
$\Delta_r G_{298}$	-1001.2	-1011.7

[a] Zero-point energy and thermal contributions calculated with the SV(P) basis set.

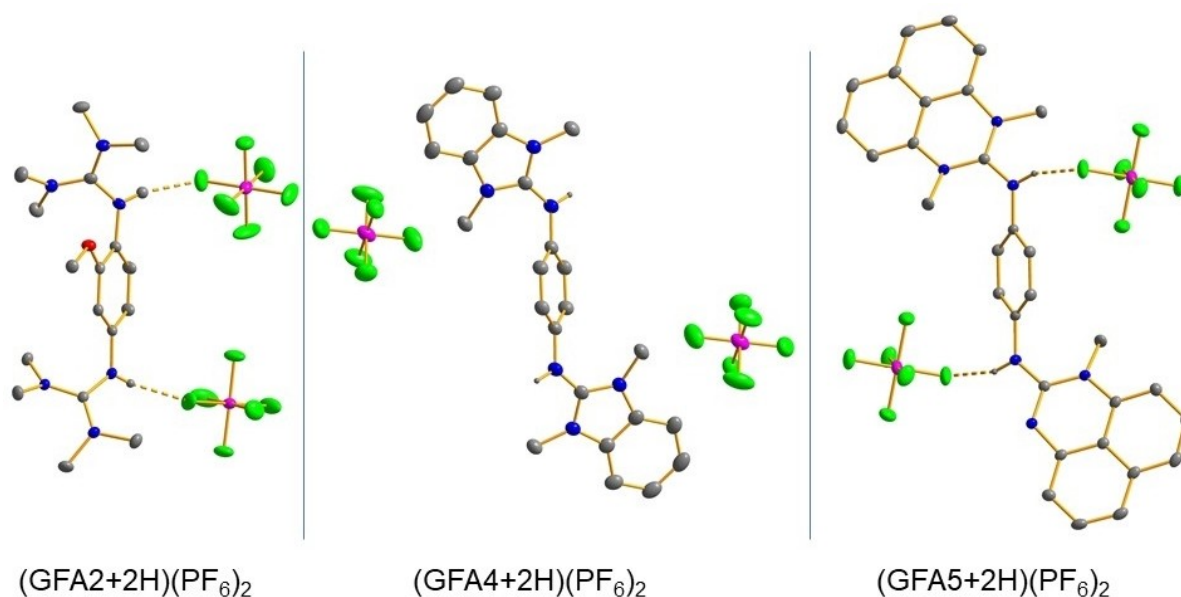


Figure 8. Illustration of the structures of the doubly protonated bisguanidines in the solid state. Displacement ellipsoids drawn at the 50% probability level. Hydrogen atoms omitted. Hydrogen bonding between the dications and the PF₆⁻ counterions is highlighted by dashed lines.

and an adjacent PF₆⁻ counterion from the experimental solid-state structures of the doubly protonated bisguanidines. A complete survey of the structures that follow from different starting geometries (different positions of the PF₆⁻ counterion around the monoprotonated bisguanidine) was not undertaken due to the immense computational cost of such a survey. Therefore, we could not completely exclude a considerable error for calculations that include anions. On the other hand,

the addition of the counterions is generally advisable in COSMO calculations.^[27,29,30]

We also calculated the thermodynamics of double-proton exchange between (GFA1+2H)(PF₆)₂ and one of the other neutral bisguanidines; the values could be obtained by subtracting the values for the proton-coupled electron transfer (PCET, see Table 7 in the next section) from the values for pure electron transfer (Table 5). A discussion follows in the next section.

Table 7. Electronic energy, enthalpy at 0 K and Gibbs free energy at 298 K for proton-coupled electron transfer reactions calculated with density functional calculations with the B3LYP functional.

	$\epsilon_r = 1$	$\epsilon_r = 37.5$	
GFA1(PF ₆) ₂ + (GFA2 + 2H)(PF ₆) ₂ → (GFA1 + 2H)(PF ₆) ₂ + GFA2(PF ₆) ₂	SV(P)	TZVP ^[a]	TZVP ^[a]
$\Delta_r E$	-41.4	-40.4	-28.0
$\Delta_r H^0$	-36.1	-35.1	-22.7
$\Delta_r G_{298}$	-28.5	-27.4	-15.0
GFA1(PF ₆) ₂ + (GFA3 + 2H)(PF ₆) ₂ → (GFA1 + 2H)(PF ₆) ₂ + GFA3(PF ₆) ₂	SV(P)	TZVP ^[a]	TZVP ^[a]
$\Delta_r E$	-82.9	-74.5	-58.0
$\Delta_r H^0$	-77.4	-69.0	-52.5
$\Delta_r G_{298}$	-66.7	-58.2	-41.8
GFA1(PF ₆) ₂ + (GFA4 + 2H)(PF ₆) ₂ → (GFA1 + 2H)(PF ₆) ₂ + GFA4(PF ₆) ₂	SV(P)	TZVP ^[a]	TZVP ^[a]
$\Delta_r E$	-58.8	-51.9	-48.6
$\Delta_r H^0$	-55.7	-48.8	-45.5
$\Delta_r G_{298}$	-44.3	-37.3	-34.1
GFA1(PF ₆) ₂ + (GFA5 + 2H)(PF ₆) ₂ → (GFA1 + 2H)(PF ₆) ₂ + GFA5(PF ₆) ₂	SV(P)	TZVP ^[a]	TZVP ^[a]
$\Delta_r E$	-54.9	-51.8	-49.4
$\Delta_r H^0$	-53.3	-50.2	-47.8
$\Delta_r G_{298}$	-49.4	-47.8	-43.4

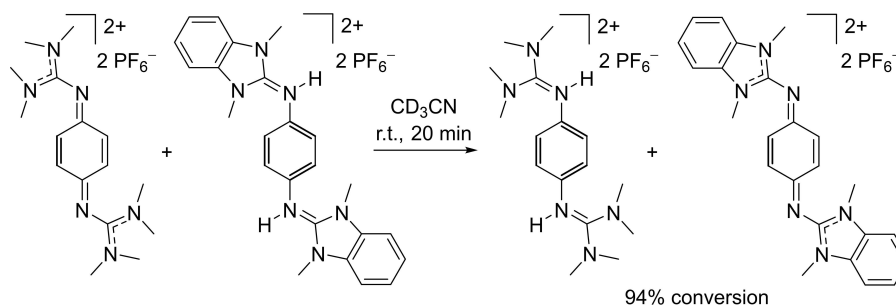
[a] Zero-point energy and thermal contributions calculated with the SV(P) basis set.

Comparative PCET reactivity

Experimental results

Next we inspected PCET reactions between the salt $\text{GFA1}(\text{PF}_6)_2$, containing the twofold-oxidized form GFA1^{2+} , with the reduced, doubly-protonated form of another bisguanidine. An example, reaction between GFA1^{2+} and $(\text{GFA4}+2\text{H})^{2+}$, is shown in Scheme 3. In all cases, GFA1^{2+} was reduced and twofold protonated to give $(\text{GFA1}+2\text{H})^{2+}$, and the reduced, twofold-protonated reaction partner deprotonated and oxidized to the dication. Hence, the results indicate that the salt $\text{GFA1}(\text{PF}_6)_2$ is the strongest oxidant in PCET reactions.

The conversion was followed by ^1H NMR spectroscopy to gain (qualitative) information about the reaction rates (see Figure 9). The reaction between GFA1^{2+} and $(\text{GFA5}+2\text{H})^{2+}$ was completed almost instantly; therefore it is not included in Figure 9. Reaction between GFA1^{2+} and $(\text{GFA4}+2\text{H})^{2+}$ required 20 min for 93% conversion under the chosen conditions. Reaction between GFA1^{2+} and $(\text{GFA3}+2\text{H})^{2+}$ was slower; 93% conversion was reached after 180 min,^[30] and 99% after 300 min. The lowest reaction rate was measured for the reaction



Scheme 3. Example PCET reaction between $\text{GFA1}(\text{PF}_6)_2$ and $(\text{GFA4}+2\text{H})(\text{PF}_6)_2$ studied to sort the five bisguanidines with respect to their PCET reactivity.

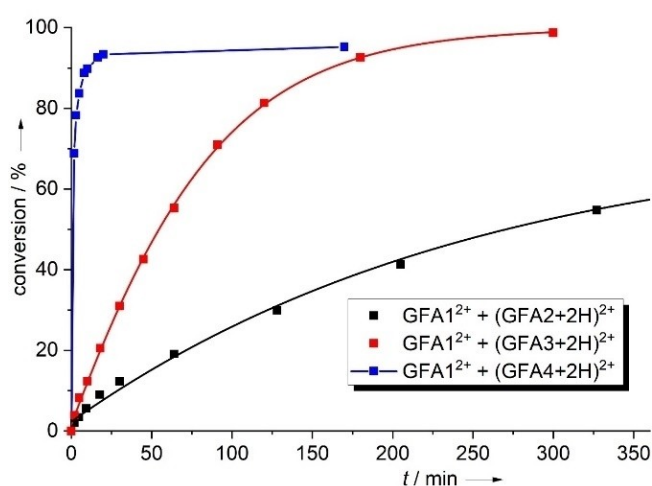


Figure 9. Comparison between the conversion vs. time plots for the reaction of $\text{GFA1}(\text{PF}_6)_2$ with the doubly-protonated, reduced forms of a second GFA in CH_3CN solution at room temperature ($c=0.015\text{ mol}\cdot\text{l}^{-1}$ for both compounds).

between GFA1^{2+} and $(\text{GFA2}+2\text{H})^{2+}$, requiring more than 800 min for 70% conversion (see Supporting Information for a complete curve). In all experiments, no reaction intermediate appeared in the NMR spectra.

Moreover, we followed the reaction between GFA1^{2+} and $(\text{GFA4}+2\text{H})^{2+}$ by UV-vis spectroscopy. The dication GFA4^{2+} formed in this reaction could easily be traced by its characteristic electronic absorption at 495 nm (Figure 10). No bands due to reaction intermediates were detected. Hence, the NMR and UV-vis spectroscopic measurements clearly show that an intermediate arising from the transfer of only one proton and/or electron is not formed in significant amount. In further UV-vis experiments, we tried to achieve pseudo-first order conditions by applying an excess of $\text{GFA1}(\text{PF}_6)_2$ (10, 20 and 40 eq.). Clearly, the rate constant increases with increasing concentration of $\text{GFA1}(\text{PF}_6)_2$ (see Supporting Information for details). However, an analysis showed that the kinetics does not follow a simple second-order rate law. The two reactants are both dications. Therefore, the approach of the two reactants to give a hydrogen-bonded complex is opposed by a strong electrostatic barrier, and also a barrier due to solvent reorganization, contributing to the overall reaction rate.

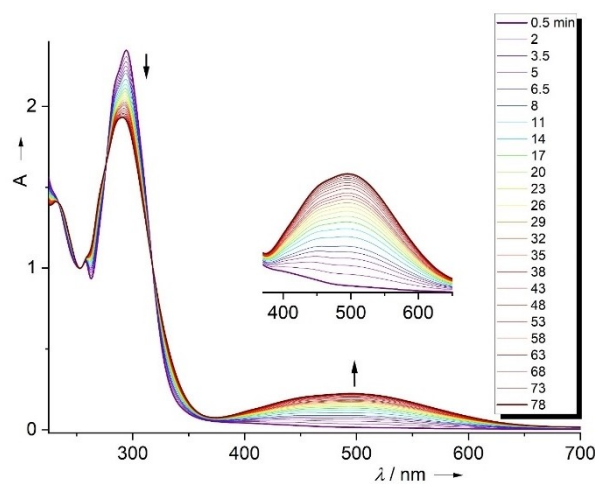


Figure 10. a) UV-vis spectra for the PCET reaction between $\text{GFA1}(\text{PF}_6)_2$ and $(\text{GFA4}+2\text{H})(\text{PF}_6)_2$ in CH_3CN at room temperature, both applied in a concentration of $4\cdot 10^{-5}\text{ mol}\cdot\text{l}^{-1}$. The reaction is completed within 80 min under the applied conditions.

Quantum-chemical calculations

Table 7 summarizes thermodynamic state functions calculated for the considered PCET reactions. The Δ_rG values for the PCET reactions between the oxidized, dicationic redox state GFA1^{2+} and the reduced, diprotonated form of another bisguanidine are included as red bars in Figure 11. In all cases, negative Δ_rG values were obtained, meaning that the reaction in which the doubly protonated, reduced bisguanidine is oxidized to the dicationic, oxidized bisguanidine is exergonic. This result is in full agreement with the experimental results showing that all these reactions take place in the predicted direction. Figure 11 directly compares the Gibbs free energy change of reactions in which only electron transfer occurs (blue bars) with reactions involving both electron and proton transfer (both at $\epsilon_r=37.5$). In the case of GFA4 and GFA5, pure electron transfer leading to oxidation of the two bisguanidines by $\text{GFA1}(\text{PF}_6)_2$ are endergonic. Nevertheless, oxidation of $(\text{GFA4}+2\text{H})^{2+}$ as well as $(\text{GFA5}+2\text{H})^{2+}$ by GFA1^{2+} via PCET are exergonic reactions, and the experiments showed that these reactions are even particularly fast. Compounds GFA4 and GFA5 are considerably weaker Brønsted bases than GFA1. The lower Brønsted basicity leads to an exergonic reaction if electron transfer is coupled with proton transfer. The high reaction rate implies that the proton-transfer step decisively contributes to the overall rate.

According to the experiments, the reaction between $(\text{GFA4}+2\text{H})(\text{PF}_6)_2$ and $\text{GFA1}(\text{PF}_6)_2$ is the slowest reaction. It also is the reaction that exhibits the highest (least negative) Gibbs free energy change. However, the experimentally observed order in the reaction rates does not fully correlate with the calculated order for the thermodynamics of the $(2e^-, 2\text{H}^+)$ PCET reactions. Hence, reaction with $(\text{GFA3}+2\text{H})^{2+}$ is slower than reaction with $(\text{GFA4}+2\text{H})^{2+}$, in opposition to the trend in the Gibbs free energy changes. This result again points to the importance of proton transfer for the reaction rate, since GFA4 is a weaker

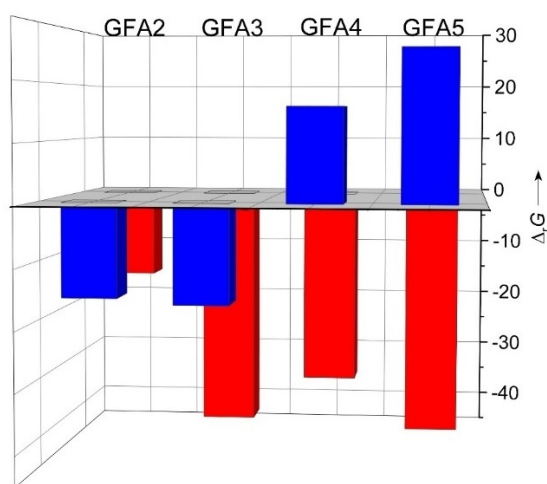


Figure 11. Comparison between the reaction Gibbs free energy Δ_rG for the oxidation of the neutral, reduced bisguanidines by $\text{GFA1}(\text{PF}_6)_2$ (dicationic, oxidized form) in a pure electron transfer reaction (blue bars) and in a PCET reaction (red bars) from B3LYP/def2-TZVP calculations with COSMO ($\epsilon_r=37.5$).

proton acceptor (see Table 6) but also a weaker electron donor (see Table 5) compared with GFA3.

In a previous study we showed that the reaction between GFA1 and 10-methyl-9,10-dihydroacridane (AcrH_2) follows a mechanism in which an electron transfer equilibrium is followed by proton transfer.^[30] Both the rate of the electron transfer step and that of the proton transfer step enter into the overall rate equation, that could be formulated as $k_{\text{H}}=k_{\text{p}}k_{\text{et}}/(k_{\text{et}}+k_{\text{p}})$, where k_{p} is the rate constant for proton transfer, and k_{et} and k_{et} are the rate constants for electron transfer and back electron transfer regenerating the reactants, respectively. Similar results were also reported for the reaction between tetrachloro-1,4-benzoquinone (chloranil) and AcrH_2 in acetonitrile.^[38] Most likely, the PCET reactions between the bisguanidines studied herein follow a similar mechanism. However, as mentioned previously, the equilibrium constant for the formation of the initial hydrogen-bond complex also enters into the rate equation, since the approach of the two dicationic reaction partners is opposed by a high barrier due to electrostatic repulsion and solvent reorganization.

In summary, the experimental and quantum-chemical results show that GFA1 is the strongest oxidant in PCET reactions of the five considered bisguanidines. However, it is not the strongest oxidant in pure electron transfer reactions, since GFA4 and GFA5 exhibit higher redox potentials.

Test reactions for applications in preparative chemistry

In the final section of this work, we demonstrate the use of the two oxidized bisguanidines GFA1^{2+} and GFA4^{2+} as PCET reactants in typical intra- and intermolecular aryl-aryl coupling reactions, and in an oxidative lactonization reaction. We selected these two bisguanidines for the following reasons: (i) GFA1^{2+} is the strongest oxidant in PCET reactions of all five considered bisguanidines. (ii) GFA4^{2+} is a stronger oxidant than GFA1^{2+} in pure electron-transfer reactions, but exhibits a lower proton affinity. By comparing the reactivity of GFA1^{2+} and GFA4^{2+} , the importance of both factors on the PCET reactivity could be analysed. (iii) GFA4^{2+} displays a characteristic band in the visible region (at 495 nm) that could be used to follow the conversion by UV-vis spectroscopy. The test reactions do not intend to demonstrate the scope of reactivity of these GFAs (see previous papers on this issue^[29,30]). The aims are to complete the analysis of the reactivity differences between GFA1 and GFA4, giving information on the reaction mechanism, and to answer the question about the required amount of acid for reaction initiation, highlighting the advantages of GFA reagents in PCET reactions with respect to high-potential quinones. We used $\text{HBF}_4 \cdot \text{OEt}_2$ as acid and CH_3CN as solvent; the Et_2O signals in the ^1H NMR spectra could be used to verify the amount of added acid. In the case of the two coupling reactions, the conversion could not be followed easily by NMR spectroscopy due to the intermediate formation of radical species. Therefore, the conversion/yield was determined after work-up (see Supporting Information for details).

Intramolecular oxidative coupling of 3,3''-4,4''-tetramethoxy-*o*-terphenyl

We already reported the reaction of GFA1(PF₆)₂ with 3,3''-4,4''-tetramethoxy-*o*-terphenyl (oxidation potential of +0.74 V vs. Fc⁺/Fc) to give the corresponding triphenylene (Table 8).^[30] Herein, we compare the reactions with GFA1(PF₆)₂ and GFA4(PF₆)₂ as PCET reagent, carried out in CH₃CN solution at room temperature. In both cases, the addition of a strong acid is needed, but only 12.5 mol% HBF₄·OEt₂ are sufficient for clean, efficient coupling. The results are summarized in the table integrated in Table 8. The conversion was determined by NMR spectroscopy after a work-up procedure yielding a mixture of the coupling product and the reduced, deprotonated bisguanidine (see Supporting Information for detailed information). Reaction with GFA1(PF₆)₂ was faster than with GFA4(PF₆)₂. With 0.13 equivalents of HBF₄·OEt₂, 88% of the coupling product was obtained after 6 h at room temperature for reaction with GFA1(PF₆)₂, but only 80% after 25 h at room temperature for reaction with GFA4(PF₆)₂. The best results were obtained for reaction at 333 K with GFA1(PF₆)₂ and 1.3 equivalents of HBF₄·OEt₂ (96% after 10 min reaction time). For comparison, reaction with 2,3-dichloro-5,6-dicyano-1,4-benzoquinone (DDQ) requires a huge amount of a strong acid (e.g. methanesulfonic acid in CH₂Cl₂ in a 1:9 v/v solvent mixture).^[39]

To show that the coupling product could be quantitatively separated from the bisguanidine, the mixture was dissolved in Et₂O and the bisguanidine protonated by addition of HCl·OEt₂ for two reactions with GFA1(PF₆)₂ and GFA4(PF₆)₂ (see Supporting Information for details) After filtration over celite the NMR spectrum of the filtrate showed the sole presence of the coupling product. The remaining residue consists of the twofold-protonated bisguanidine, that could be dissolved in CH₃CN (and re-oxidized to the PCET reagent if desired).

Intermolecular oxidative coupling of *N*-ethylcarbazole

An *E*_{1/2} value of +1.12 V vs. SCE (+0.66 V vs. Fc⁺/Fc) was measured for *N*-ethylcarbazole. Venkatakrishnan et al. showed

that reaction of DDQ or chloranil with *N*-ethylcarbazole gives quantitative conversion (>99%) of the bicarbazole coupling product (reaction in Scheme 4) in very short time when carried out in CH₂Cl₂ solution; however the addition of a large excess of methanesulfonic acid was required (1:10 v/v methanesulfonic acid:CH₂Cl₂ solvent mixture).^[40] In the reactions with GFA1 and GFA4, addition of only 1.25 eq. of an acid (HBF₄·OEt₂) was required. The reactions were carried out in CH₃CN at room temperature. After 30 min reaction time and a work-up procedure (see Supporting Information for details), the bicarbazole coupling product was obtained in excellent conversion of 97% for reaction with GFA1(PF₆)₂ and 98% for reaction with GFA4(PF₆)₂.

Oxidative lactonization of 2-[(4-methoxyphenyl)methyl]-benzoic acid

Finally, we tested the oxidative lactonization of 2-[(4-methoxyphenyl)methyl]-benzoic acid to give 3-(4-methoxyphenyl)-1(3*H*)-isobenzofuranone. This reaction was shown to proceed in high (NMR) yield with tetrachloro-*o*-benzoquinone (Q^{Cl}, Table 9) in the presence of a hydrogen-bond donor or a redox catalyst. Nocera, Jacobsen et al. reported reaction with 1.3 equivalents of the benzoquinone and several different hydrogen-bond donor compounds in CH₂Cl₂ solution at 4 °C; the best results (98% NMR yield after 24 h) were obtained with 0.1 eq. of the hydrogen-bond donor HBD sketched in Table 9.^[41] Greb et al. used 1.3 equivalents of Q^{Cl} in combination with 0.1 equivalents of the special silicon redox catalyst Si(Cat^{Cl})(SQ^{Cl})₂ (see Table 9) to obtain >95% NMR yield, again in CH₂Cl₂ at 4 °C after 24 h reaction time.^[42] Moreover, a photo-catalytic reaction in CH₃CN solution at room temperature with 5 mol% DDQ and 50 mol% tert-butyl nitrite was reported, using dioxygen from air as terminal oxidant.^[43] The mixture was irradiated for 24 h by a blue compact fluorescent lamp with λ = 450 ± 50 nm light. The conversion was high, but a mixture of the phthalide product together with the hydroxylated phthalide was obtained.^[43]

In our initial experiments, we used one equivalent of GFA1(PF₆)₂ or GFA4(PF₆)₂, and also one equivalent of HBF₄·OEt₂

Table 8. Intramolecular aryl-aryl coupling reaction of 3,3''-4,4''-tetramethoxy-*o*-terphenyl. The stated conversion was determined after work-up, leading to a mixture of the coupling product and the reduced, twofold-protonated GFA from which the coupling product could be quantitatively separated by filtration over celite (see Supporting Information for details).

PCET reagent	eq. of HBF ₄ ·OEt ₂	temperature/time	conversion
GFA1(PF ₆) ₂	0.13	298 K, 6 h	88%
GFA1(PF ₆) ₂	1.3	333 K, 10 min	96%
GFA4(PF ₆) ₂	0.13	298 K, 6 h	63%
GFA4(PF ₆) ₂	0.13	298 K, 25 h	80%
GFA4(PF ₆) ₂	1.1	298 K, 1.5 h	86%

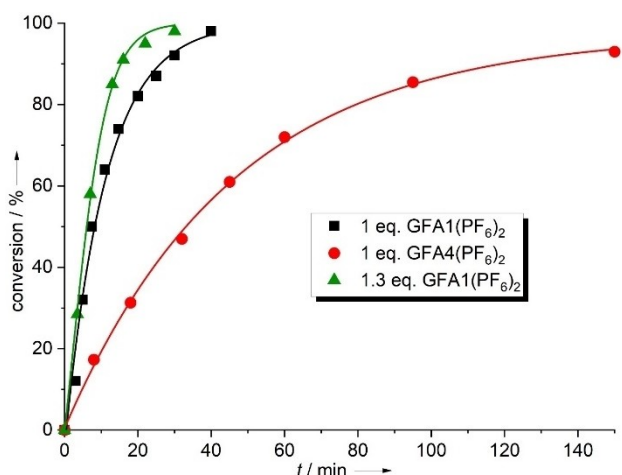


Figure 12. Conversion vs. time plots for lactonization of 2-[(4-methoxyphenyl)methyl]-benzoic acid with GFA1(PF₆)₂ or GFA4(PF₆)₂, from NMR spectroscopic measurements. See Supporting Information for the complete curve with 1 eq. GFA4(PF₆)₂.

ments also confirm the importance of the rate for proton transfer for the overall reaction rate.

As expected, an increase of the temperature to 60 °C led to a decrease of the reaction time for quantitative conversion (see Table 9). Finally, the reaction was repeated with 1.3 equivalents of GFA1(PF₆)₂ (see Table 9 and Figure 12, green curve). The reaction proceeded faster than with 1.0 equivalent (quantitative conversion after 30 min), confirming that the concentration of the PCET reagent enters into the rate equation (see the discussion above).

Conclusions

Proton-coupled electron transfer (PCET) is of immense importance in redox-enzymatic reactions in biology and also in synthetic chemistry. In this work we analyse the effect of modifications at the guanidino groups and the aromatic core on the PCET properties of redox-active bisguanidines. For this systematic study, a series of five 1,4-bisguanidino-benzene derivatives was considered. First, the new molecules were synthesized and characterized in all relevant charge and protonation states. The analysis of the redox potentials and proton affinities showed that the driving force for PCET reactions is either the electron transfer (redox) step or the proton transfer step. Thereby, comparative PCET reactions between the five bisguanidines provided (qualitative) information about the mechanisms of PCET reactions. Interestingly, comparative reactions, being endergonic in the case of pure electron transfer, turned to be most exergonic with fastest conversion if electron transfer is accompanied with proton transfer. The differences in the Brønsted basicities explain these results, highlighting their decisive role for the thermodynamics and demonstrating the important contribution of the proton transfer step for the overall reaction rates. The results of our

combined experimental and quantum-chemical analysis clearly decode the importance of the two parameters, redox potential and Brønsted basicity, for the PCET properties of redox-active bisguanidines, and depict the possibilities for their fine tuning.

Finally, two bisguanidino-benzene compounds were applied in typical intra- and intermolecular aryl-aryl coupling reactions and in an oxidative lactonization. All these reactions proceeded almost quantitatively at mild conditions. The amount of acid that was needed to initiate the reactions (one or even only 0.13 equivalents) was much lower than in traditional procedures relying on high-potential quinones. Hence, the results of this work demonstrate the huge potential of redox-active guanidines as valuable alternatives to toxic high-potential quinones for use as PCET reagents.

Acknowledgements

The authors gratefully acknowledge continuous financial support by the German research foundation (DFG). We thank M. Sc. Rezisha Maskey for giving us some 2-[(4-methoxyphenyl)methyl]-benzoic acid. Open access funding enabled and organized by Projekt DEAL.

Conflict of Interest

The authors declare no conflict of interest.

Keywords: C–H activation · guanidines · proton affinity · proton-coupled electron transfer · redox potential

- [1] M. H. V. Huynh, T. J. Meyer, *Chem. Rev.* **2007**, *107*, 5004–5064.
- [2] D. R. Weinberg, C. J. Gagliardi, J. F. Hull, C. F. Murphy, C. A. Kent, B. C. Westlake, A. Paul, D. H. Ess, D. G. McCafferty, T. J. Meyer, *Chem. Rev.* **2012**, *112*, 4016–4093.
- [3] J. J. Warren, T. A. Tronic, J. M. Mayer, *Chem. Rev.* **2010**, *110*, 6961–7001.
- [4] D. R. Weinberg, C. J. Gagliardi, J. F. Hull, C. F. Murphy, C. A. Kent, B. C. Westlake, A. Paul, D. H. Ess, D. G. McCafferty, T. J. Meyer, *Chem. Rev.* **2012**, *112*, 4016–4093.
- [5] I. Siewert, *Chem. Eur. J.* **2015**, *21*, 15078–15091.
- [6] E. C. Gentry, R. R. Knowles, *Acc. Chem. Res.* **2016**, *49*, 1546–1556.
- [7] D. C. Miller, K. T. Tarantino, R. R. Knowles, *Top. Curr. Chem.* **2016**, *374*:30.
- [8] H. G. Yayla, R. R. Knowles, *Synlett* **2014**, *25*, 2819–2826.
- [9] Proton-Coupled Electron Transfer, A Carrefour of Chemical Reactivity Traditions, *RSC Catalysis Series*, Eds. Formosinho, S.; Barroso, M. RSC Publishing. Royal Society of Chemistry **2012**.
- [10] S. Y. Reece, D. G. Nocera, *Annu. Rev. Biochem.* **2009**, *78*, 673–699.
- [11] S. Y. Reece, J. M. Hodgkiss, J. Stubbe, D. G. Nocera, *Phil. Trans. R. Soc. B* **2006**, *361*, 1351–1364.
- [12] A. Migliore, N. F. Polizzi, M. J. Therien, D. N. Beratan, *Chem. Rev.* **2014**, *114*, 3381–3465.
- [13] V. R. I. Kaila, M. I. Verkhovskiy, M. Wikström, *Chem. Rev.* **2010**, *110*, 7062–7081.
- [14] a) M. D. Tzirakis, I. N. Lykakis, M. Orfanopoulos, *Chem. Soc. Rev.* **2009**, *38*, 2609–2621; b) D. Ravelli, S. Protti, M. Fagnoni, *Acc. Chem. Res.* **2016**, *49*, 2232–2242; c) D. Ravelli, M. Fagnoni, T. Fukuyama, T. Nishikawa, I. Ryu, *ACS Catal.* **2018**, *8*, 701–713; d) G. Laudadio, Y. Deng, K. van der Wal, D. Ravelli, M. Nuño, M. Fagnoni, D. Guthrie, Y. Sun, T. Noël, *Science* **2020**, *369*, 92–96.
- [15] a) D. Walker, J. D. Hiebert, *Chem. Rev.* **1967**, *67*, 153–195; b) S. B. Bharate, *Synlett* **2006**, 496–497.
- [16] J. Piera, J.-E. Bäckvall, *Angew. Chem. Int. Ed.* **2008**, *47*, 3506–3523; *Angew. Chem.* **2008**, *120*, 3558–3576.

- [17] M. T. Huynh, C. W. Anson, A. C. Cavell, S. S. Stahl, S. Hammes-Schiffer, *J. Am. Chem. Soc.* **2016**, *138*, 15903–15910.
- [18] S. Lerch, L.-N. Unkel, P. Wienefeld, M. Brasholz, *Synlett* **2014**, *25*, 2673–2680.
- [19] Q. Cao, L. M. Doman, L. Rogan, N. L. Hughes, M. J. Muldoon, *Chem. Commun.* **2014**, *50*, 4524–4543.
- [20] F. Wang, S. S. Stahl, *Acc. Chem. Res.* **2020**, *53*, 561–574.
- [21] R. Ciriminna, M. Pagliaro, *Org. Process Res. Dev.* **2010**, *14*, 245–251.
- [22] B. L. Ryland, S. S. Stahl, *Angew. Chem. Int. Ed.* **2014**, *53*, 8824–8838; *Angew. Chem.* **2014**, *126*, 8968–8983.
- [23] C. Zheng, S.-L. You, *Chem. Soc. Rev.* **2012**, *41*, 2498–2518.
- [24] W. Huang, X. Cheng, *Synlett* **2017**, *28*, 148–158.
- [25] H.-J. Himmel, *Synlett* **2018**, *29*, 1957–1977.
- [26] U. Wild, S. Federle, A. Wagner, E. Kaifer, H.-J. Himmel, *Chem. Eur. J.* **2016**, *22*, 11971–11976.
- [27] U. Wild, O. Hübner, L. Greb, M. Enders, E. Kaifer, H.-J. Himmel, *Eur. J. Org. Chem.* **2018**, 5910–5915.
- [28] U. Wild, F. Schön, H.-J. Himmel, *Angew. Chem. Int. Ed.* **2017**, *56*, 16410–16413; *Angew. Chem.* **2017**, *129*, 16630–16633.
- [29] U. Wild, O. Hübner, H.-J. Himmel, *Chem. Eur. J.* **2019**, *25*, 15988–15992.
- [30] U. Wild, P. Walter, O. Hübner, E. Kaifer, H.-J. Himmel, *Chem. Eur. J.* **2020**, *26*, 16504–16513.
- [31] A. Peters, E. Kaifer, H.-J. Himmel, *Eur. J. Org. Chem.* **2008**, 5907–5914.
- [32] B. Eberle, O. Hübner, A. Ziesak, E. Kaifer, H.-J. Himmel, *Chem. Eur. J.* **2015**, *21*, 8578–8590.
- [33] J. Hornung, O. Hübner, E. Kaifer, H.-J. Himmel, *RSC Adv.* **2016**, *6*, 39323–39329.
- [34] S. Dorok, *Eur. Pat. Appl.* 2963010, **2016**.
- [35] M. Werr, E. Kaifer, H. Wadepohl, H.-J. Himmel, *Chem. Eur. J.* **2019**, *25*, 12981–12990.
- [36] R. Gleiter, J. Uschmann, *J. Org. Chem.* **1986**, *51*, 370–380.
- [37] Deposition Number(s) 2078036 (for GFA2), 2078037 (for (GFA2+2H)(PF₆)₂), 2078031 (for GFA4), 2078032 (for (GFA4+2H)(PF₆)₂), 2078033 (for GFA4(PF₆)₂), 2078034 (for (GFA5+2H)(PF₆)₂), and 2078035 (for GFA5(PF₆)₂) contain(s) the supplementary crystallographic data for this paper. These data are provided free of charge by the joint Cambridge Crystallographic Data Centre and Fachinformationszentrum Karlsruhe Access Structures service www.ccdc.cam.ac.uk/structures.
- [38] S. Fukuzumi, H. Kotani, Y.-M. Lee, W. Nam, *J. Am. Chem. Soc.* **2008**, *130*, 15134–15142.
- [39] a) L. Zhai, R. Shukla, R. Rathore, *Org. Lett.* **2009**, *11*, 3474–3477; b) L. Zhai, R. Shukla, S. H. Wadumethrige, R. Rathore, *J. Org. Chem.* **2010**, *75*, 4748–4760.
- [40] S. Mallick, S. Maddala, K. Kollimalayan, P. Venkatakrishnan, *J. Org. Chem.* **2019**, *84*, 73–93.
- [41] A. K. Turek, D. J. Hardee, A. M. Ulman, D. G. Nocera, E. N. Jacobsen, *Angew. Chem. Int. Ed.* **2016**, *55*, 539–544; *Angew. Chem.* **2016**, *128*, 549–554.
- [42] R. Maskey, C. Bendel, J. Malzacher, L. Greb, *Chem. Eur. J.* **2020**, *26*, 17386–17389.
- [43] F. Rusch, J.-C. Schober, M. Brasholz, *ChemCatChem* **2016**, *8*, 2881–2884.

Manuscript received: April 30, 2021
Accepted manuscript online: June 16, 2021
Version of record online: July 8, 2021